Volcanic Initiation of the Eocene Heart Mountain Slide, Wyoming, USA

David H. Malone,[1,*] John P. Craddock,[2] Mark D. Schmitz,[3] Stuart Kenderes,[4] Ben Kraushaar,[5] Caelan J. Murphey,[1] Stefan Nielsen,[6] and Thomas M. Mitchell[7]

1. Department of Geography-Geology, Illinois State University, Normal, Illinois 61790, USA; 2. Geology Department, Macalester College, St. Paul, Minnesota 55105, USA; 3. Department of Geosciences, Boise State University, Boise, Idaho 83725, USA; 4. Department of Geological Sciences, University of Missouri, Columbia, Missouri 65211, USA; 5. Department of Geology and Geophysics, University of Wyoming, Laramie, Wyoming 82701, USA; 6. Department of Earth Sciences, Durham University, Durham DH13LE, United Kingdom; 7. Department of Earth Sciences, University College London, London, United Kingdom

ABSTRACT

The Eocene Heart Mountain slide of northwest Wyoming covers an area of as much as 5000 km² and includes allochthonous Paleozoic carbonate and Eocene volcanic rocks with a run-out distance of as much as 85 km. Recent geochronologic data indicated that the emplacement of the slide event occurred at ~48.9 Ma, using laser ablation inductively coupled plasma mass spectrometry (LA-ICPMS) extracted from U-Pb zircon ages from basal layer and injectite carbonate ultracataclasite (CUC). We now refine that age with U-Pb results from a lamprophyre diatreme that is temporally and spatially related to the CUC injectites. The ages for the lamprophyre zircons are 48.97 ± 0.36 Ma (LA-ICPMS) and 49.19 ± 0.02 Ma (chemical abrasion isotope dilution thermal ionization mass spectrometry). Thus, the lamprophyre and CUC zircons are identical in age, and we interpret that the zircons in the CUC were derived from the lamprophyre during slide emplacement. Moreover, the intrusion of the lamprophyre diatreme provided the trigger mechanism for the Heart Mountain slide. Additional structural data are presented for a variety of calcite twinning strains, results from anisotropy of magnetic susceptibility for the lamprophyre and CUC injectites and alternating-field demagnetization on the lamprophyre, to help constrain slide dynamics. These data indicate that White Mountain experienced a rotation about a vertical axis and minimum of 35° of counterclockwise motion during emplacement.

Online enhancements: supplemental tables.

Introduction

The Heart Mountain slide has been one of the most controversial and enigmatic features in North America for nearly 120 y. The slide covers an area of at least 3500 km² (Hauge 1993 and references therein) and perhaps as much as 5000 km², with a run-out distance of as much as 85 km (Malone et al. 2014b). White Mountain is one of the best exposures of the Heart Mountain slide and is an allochthon of Paleozoic carbonate and Eocene volcanic rocks. The western half of White Mountain, which is in the distal portion of the bedding-parallel section of the Heart Mountain slide, is the only occurrence of marble within the entire Heart Mountain system. This thermal metamorphism took place before slide emplacement and likely accompanied intrusion of the diorite stock at the northeast end of White Mountain (Malone et al. 2014a).

The base of allochthonous rocks at White Mountain is defined by a horizontal, 2-m-thick carbonate

ultracataclasite (CUC; Craddock et al. 2009) that fed eight injectites of the same material, which are as much as 120 m above the slide base within marble and Madison Group limestones (Craddock et al. 2012). Existing structural, mineralogical, and geochemical constraints indicate that the Heart Mountain slide moved at ~100 m/s (Craddock et al. 2009).

New field and lab work has identified a coeval tabular lamprophyre dike (striking N55°E) at White Mountain that is the remnant of a lamprophyre diatreme that may have triggered the Heart Mountain slide. We present calcite twinning-strain, AMS (anisotropy of magnetic susceptibility), paleomagnetic, compositional, petrological, and geochronologic data

on this lamprophyre to unravel the details of the relationship of emplacement kinematics and mechanics of the Heart Mountain slide.

Previous Work

The Heart Mountain slide is one of the largest subaerial landslides on Earth, with the only analog being the 21 Ma Markagunt slide in Utah (Hacker et al. 2014). The Heart Mountain slide initiated on a 50-km-long, gently dipping bedding plane within the Ordovician Bighorn Dolomite, cutting upsection for ~5 km and out onto the Eocene landscape (Malone et al. 2014a; figs. 1–3). Most of those working
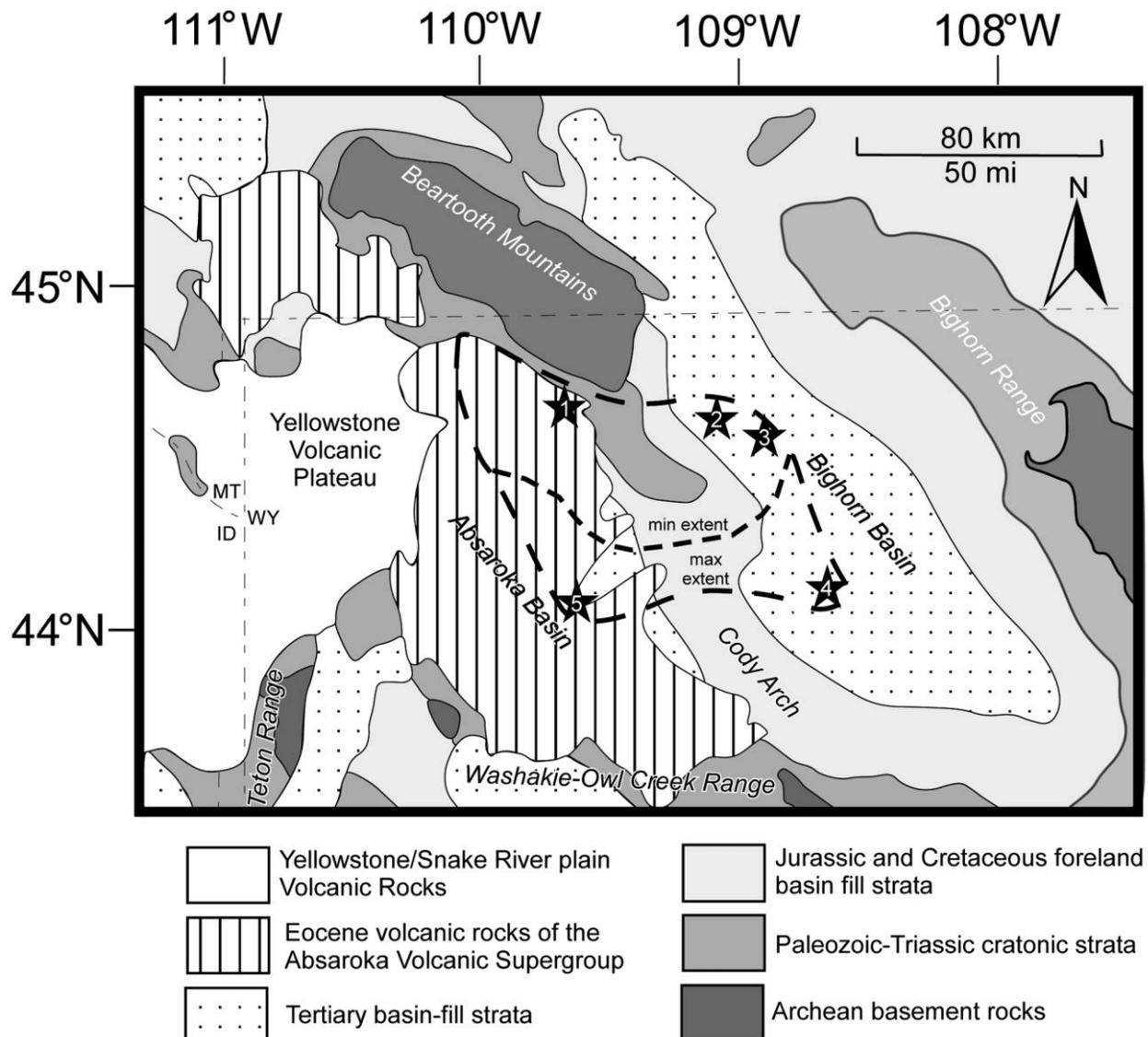
Figure 1. Generalized geologic map of northwest Wyoming, illustrating the areal extent of the Heart Mountain slide and locations of features discussed in the text. 1 = White Mountain, 2 = Heart Mountain, 3 = McCullough Peaks, 4 = Squaw Peaks, 5 = Upper South Fork Shoshone River Valley. Modified from Malone et al. (2014b, 2014c).
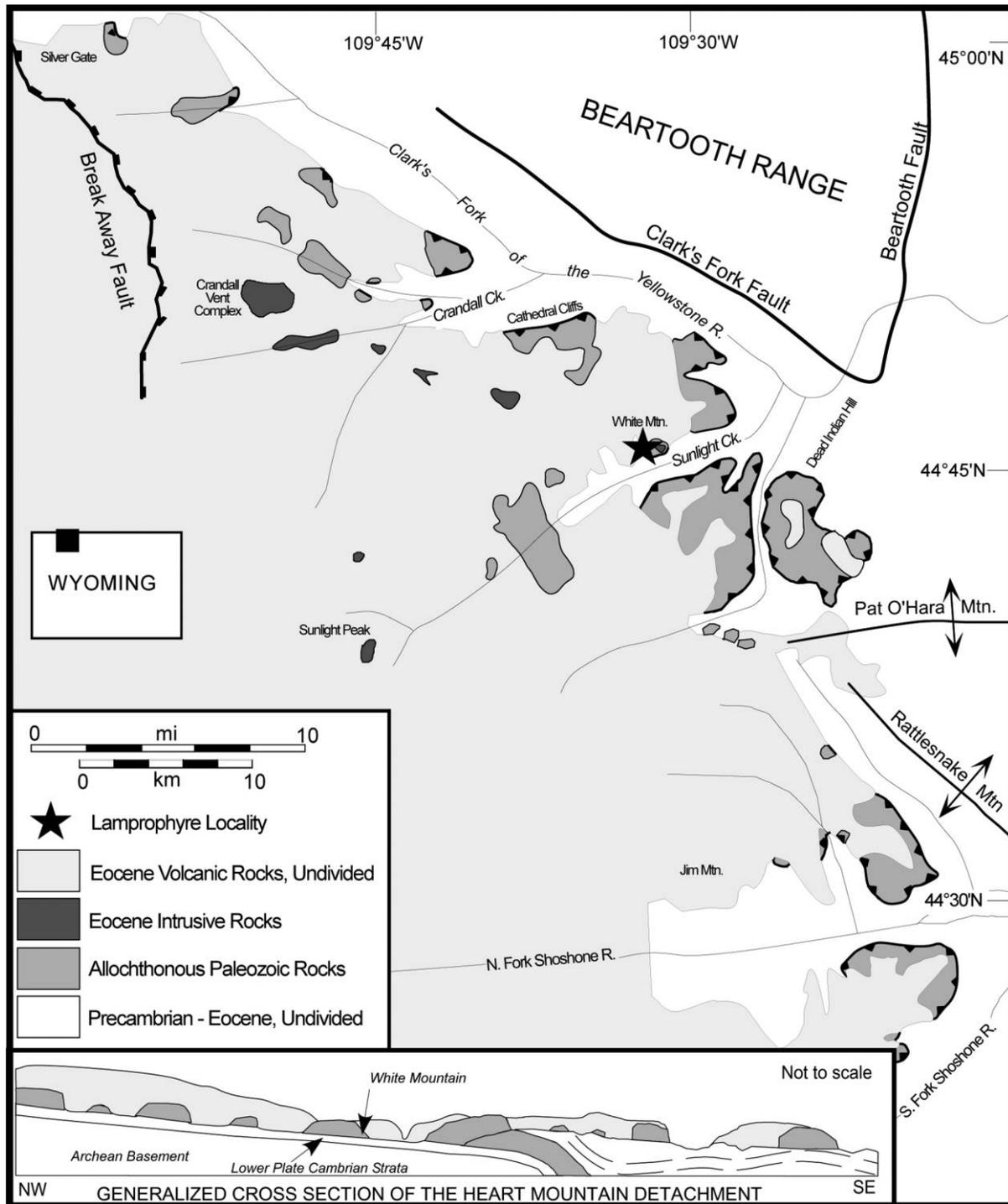
Figure 2. Generalized geologic map of the Heart Mountain slide area. Modified from Hauge (1993) and Malone et al. (2014*a*).

on the slide regard it as a catastrophic event associated with widespread igneous activity in the Eocene Absaroka volcanic province (e.g., Bucher 1947; Nelson and Pierce 1968; Pierce 1973; Malone 1995; Beutner and Craven 1996; Beutner and Gerbi 2005;

Aharanov and Anders 2006; Craddock et al. 2009, 2012; Anders et al. 2010; Malone et al. 2014*a*). Timing relations are key to understanding various emplacement models, which include a catastrophic landslide followed by volcanic burial (Pierce 1973),
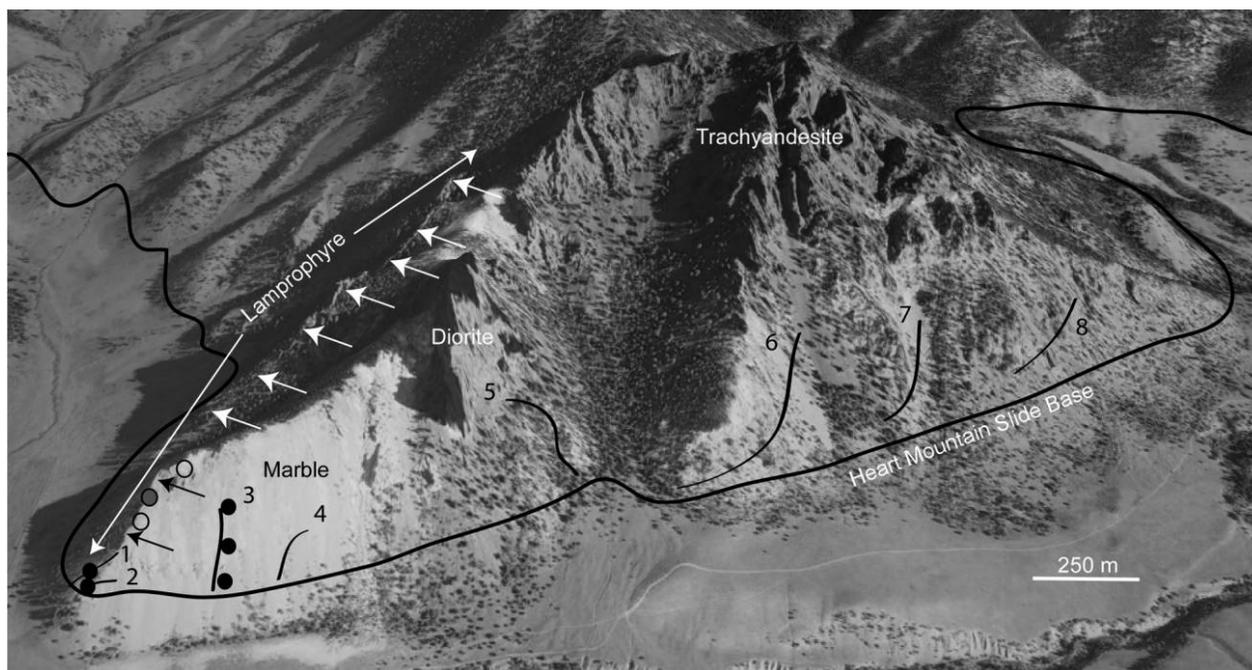
Figure 3. Oblique view of White Mountain and the basal detachment of the Heart Mountain slide, including the positions of the carbonate ultracataclasite (CUC) injectites and lamprophyre. Injectites are numbered 1–8 from west to east. Open circles indicate calcite twin samples, black circles CUC injectite AMS samples, and the gray circle the lamprophyre AMS and paleopole sample. Sample sites are indicated in subsequent figures. A color version of this figure is available online.

incremental movement potentially lasting millions of years (Hauge 1985, 1990; Templeton et al. 1995; Swanson et al. 2016), and catastrophic emplacement of Paleozoic carbonate and Eocene volcanic rocks over a period of minutes to hours (Craddock et al. 2009). The mechanism of upper-plate movement that allows for catastrophic emplacement along a low-angle surface with only minor associated deformation preserved above, along, or below the detachment is poorly understood. Contemporaneous dike intrusion (Aharanov and Anders 2006; DeFrates et al. 2006; King et al. 2009), various detachment fluids (Templeton et al. 1995; Aharanov and Anders 2006; King et al. 2009), and CO_2 generation by limestone-on-limestone sintering (Beutner and Gerbi 2005; Craddock et al. 2009; Anders et al. 2010; Mitchell et al. 2015) have been proposed to facilitate movement of the slide mass. Hauge (1993) provides an excellent detailed summary of all aspects of the first century of Heart Mountain research. Malone and Craddock (2008) summarized the research conducted from 1990 to 2008.

Throughout the proximal areas of the Heart Mountain slide, carbonate-dominated cataclastic material (first reported by Pierce 1979; referred to as CUC

in Craddock et al. 2009, 2012; previous workers have referred to this as breccia, microbreccia, or the "basal layer") occurs as a centimeters-to-meter-thick veneer along the contact of allochthonous and autochthonous rocks. The basal layer is best exposed at White Mountain (Nelson et al. 1972), along with discordant injectite dikes of the same material found up to 120 m above the slide base (Craddock et al. 2012). U-Pb ages from zircons extracted from the basal-layer CUC and injectites (White Mountain and Silver Gate) yield an age of ~48.9 Ma (Malone et al. 2014*a*).

The purpose of this article is to provide additional constraints on the timing and duration of the Heart Mountain slide, using U-Pb geochronology, magnetic, and structural techniques on rocks formed during emplacement. We describe and interpret a newly discovered lamprophyre igneous suite at White Mountain that bears on the Heart Mountain problem, and we present an analysis of the lamprophyre diatreme and slide dynamics. Thus, this work is a follow-up to Malone et al. (2014*a*), who directly tested the rapid- and gradual-emplacement hypotheses. Field evidence indicates that the lamprophyre igneous suite is geometrically and temporally related to the CUC inject-

ites at White Mountain. The concept presented and argued here is that the emplacement/eruption of the lamprophyre suite may have provided the elusive triggering mechanism for slide emplacement.

Methods

The igneous-suite energy-dispersive X-ray fluorescence (XRF) data were collected at Western Kentucky University and the Illinois State Geological Survey (table S1; tables S1–S6 available online). Mineral separations and heavy-mineral analysis via wavelength-dispersive X-ray spectroscopy on a scanning electron microscope were done at Macalester College. Fabric analysis via electron backscatter diffraction (EBSD) was done at the University of Minnesota-Duluth. Zircon crystals were analyzed for trace-element concentrations and U-Pb age via laser ablation–inductively coupled plasma mass spectrometry (LA-ICPMS) and subsequently dated at high precision by chemical abrasion–isotope dilution thermal ionization mass spectrometry (CA-IDTIMS) at Boise State University. Diamonds were analyzed with Raman spectroscopy at Western Kentucky University and X-ray diffraction and electron microprobe analysis at the University of Minnesota. Paleomagnetic measurements were conducted at the University of Minnesota Institute of Rock Magnetism. Calcite twinning-strain analysis was conducted at Macalester College.

Zircon Geochronology. In situ zircon U-Th-Pb isotope and trace-element concentration measurements were conducted at Boise State University with a ThermoElectron X-Series II quadrupole ICPMS and a New Wave Research UP-213 Nd:YAG ultraviolet (213-nm) laser ablation system. Lamprophyre breccia zircons were analyzed with a suite of standards including a large zircon megacryst from the Orapa kimberlite as a reference material. Zircons were ablated with a laser diameter of 25 μm using fluence and pulse rates of 5–6 J/cm^2 and 10 Hz, respectively, during a 45-s analysis (15-s gas blank, 30-s ablation), which excavated a pit approximately 25 μm deep. Ablated material was carried by a 1-L/min He gas stream to the plasma. Dwell times were 5 ms for Si and Zr; 40 ms for ^{49}Ti, ^{238}U, ^{232}Th, ^{202}Hg, and all Pb isotopes; and 10 ms for all other high-field-strength elements and rare earth elements (REEs). Background count rates for each analyte were obtained before each spot analysis and subtracted from the raw count rate for each analyte. For concentration calculations, background-subtracted count rates for each analyte were internally normalized to ^{29}Si and calibrated with respect to National Institute of Standards 610 and 612 glasses as the primary standards. Temper-

ature was calculated from the Ti-in-zircon thermometer (Watson et al. 2006), with a nominal activity of TiO$_2$ of 0.6 used for both lamprophyre breccia zircons and the Orapa kimberlite zircon standard.

For U-Th-Pb age analysis, instrumental fractionation of the ^{206}Pb/^{238}U, ^{207}Pb/^{206}Pb, and ^{208}Pb/^{232}Th ratios was corrected and ages calibrated with respect to interspersed measurements of the Plešovice zircon standard (Sláma et al. 2008). Signals at mass 204 are indistinguishable from 0 for most zircons after subtraction of mercury backgrounds measured during the gas blank (<150 counts/s ^{202}Hg); thus, ages are normally reported without common-Pb correction, although our data acquisition and reduction scheme allows for a variety of ^{204}Pb-, ^{207}Pb-, or ^{208}Pb-based corrections. Radiogenic-isotope ratio and age error propagation includes uncertainty contributions from counting statistics, background subtraction, and regression errors. Standard calibration uncertainty is propagated in quadrature following group statistics (e.g., weighted mean calculations); standard calibration uncertainties (2σ) over an experiment range from 1% to 2% for ^{206}Pb/^{238}U and from 0.5% to 1% for ^{207}Pb/^{206}Pb. The LA-ICPMS U-Pb isotope and trace-element results are reported in tables S2 and S3.

For more precise dates, the same zircon crystals were analyzed via CA-IDTIMS at Boise State University (table S4). Selected zircon crystals were removed from the epoxy mount and annealed at 900°C for 60 h. Individual crystal fragments were then "chemically abraded" in 120 μL of 29 M HF for 12 h at 190°C in 300-μL Teflon perfluoroalkoxy (PFA) microcapsules. The residual crystals after this partial dissolution were fluxed in 3.5 M HNO$_3$ in an ultrasonic bath and on a warm hotplate for 60 min and then rinsed twice in ultrapure H$_2$O before being reloaded into microcapsules and spiked with the mixed U-Pb isotope tracer ET535 (Condon et al. 2015). Additional details of chemical separations, mass spectrometry, and data analysis are described in Rivera et al. (2013). Errors on CA-IDTIMS U-Pb isotope ratios and dates are reported at the 95% confidence interval (2σ) in table S4. Uncertainty in the weighted mean date is given as $\pm x(y)[z]$, where x is the internal error based on analytical uncertainties only, including counting statistics, subtraction of tracer solution, and blank and initial common-Pb subtraction; y includes the tracer calibration uncertainty propagated in quadrature; and z includes the ^{238}U decay constant uncertainty propagated in quadrature. The latter uncertainty should be considered when comparing our dates with those derived from other decay schemes, such as ^{40}Ar/^{39}Ar. The resulting interpreted ages are shown on Pb*/U

concordia and ranked-age diagrams using the routines in Isoplot (Ludwig 2008).

AMS and Demagnetization Techniques. The "Roly-Poly" is an AC susceptibility bridge with an automated sample handler for determining anisotropy of low-field magnetic susceptibility at room temperature. An alternating current in the external "drive" coils produces an alternating magnetic field in the sample space with a frequency of 680 Hz and an amplitude of up to 1 mT. The induced magnetization of a sample is detected by a pair of "pickup" coils, with a sensitivity of 1.2×10^{-6} SI volume units. For anisotropy determination, a sample is rotated about three orthogonal axes, and susceptibility is measured at 1.8° intervals in each of the three measurement planes. The susceptibility tensor is computed by least squares from the resulting 600 directional measurements. Very high precision results from the large number of measurements; in most cases principal-axis orientations are reproducible to within 2° and axial ratios to within about 1%. For each measured core, one unique magnetic ellipsoid is produced and plotted. Sample anisotropy percentages ranged from 5% to 14% for the eight samples and 193 cores taken from the CUC injectites, CUC basal layer, and lamprophyre. The AMS data are provided in table S5.

Calcite Twin Analysis. The calcite strain-gage technique (CSGT) of Groshong (1972) allows investigation of intraplate stresses as constrained by intracrystalline twinning of rock-forming calcite grains. Although the result is a strain tensor, a similar orientation of the stress tensor appears likely in case of coaxial deformation (Turner 1953, 1962). The CSGT has been used to constrain strain tensor directions in veins (Kilsdonk and Wiltschko 1988; Paulsen et al. 2014), limestones (Engelder 1979; Spang and Groshong 1981; Wiltschko et al. 1985; Craddock and van der Pluijm 1988; Mosar 1989; Ferrill 1991; Craddock et al. 2000), marble (Craddock et al. 1991), amygdaloidal basalts (Craddock and Pearson 1994; Craddock et al. 1997, 2004), and lamprophyres (Craddock et al. 2007).

Below temperatures of ca. 200°C, intracrystalline deformation of calcite results in the formation of e-twins. The formation of calcite e-twins requires a shear stress exceeding ca. 10 MPa (Wenk et al. 1987; Burkhard 1993; Lacombe and Laurent 1996; Ferrill 1998). Calcite offers three glide systems for e-twinning. From U-stage measurements of width, frequency, and orientation of twins and the crystallographic orientation of the host crystals, a strain tensor can be calculated with a least squares technique (Groshong 1972). In order to remove "noise" from the data set, a refinement of the calculated strain tensor can be achieved by stripping the 20% of twins with

highest deviations (Groshong et al. 1984). This procedure has been used if the number of measured grains was large ($n > 20$). In cases where the data appear to be inhomogeneous, the separation of incompatible twins (negative expected values [NEVs]) from compatible twins (positive expected values) of the initial data set allows separate calculation of two or more least squares deviatoric-strain tensors. Thus, the CSGT can be used to obtain information on superimposed deformations (Groshong 1972, 1974) and differential stress magnitudes (Rowe and Rutter 1990).

The validity of this stripping procedure was demonstrated in experimental tests where the reliability depends on the overall complexity of deformation and the number of grains with twins (Groshong 1974; Teufel 1980). The stripping procedure was used in cases of high proportions of NEVs and a large number of measured grains. An experimental reevaluation of the CSGT has shown that measurements of about 50 grains on one thin section or 25 grains on two mutually perpendicular thin sections yield the best results (Groshong et al. 1984; Evans and Groshong 1994; Ferrill et al. 2004). The chance to extract the records of more than two deformations from one data set is limited when dealing with natural rocks (Burkhard 1993). Individual analyses of veins, matrix, nodules, and so on allows the acquisition of several strain tensors without applying statistical data stripping. The complexity of rotational strains in fault zones has limited the application of this method to the efforts of Gray et al. (2005). Application of the CSGT requires the following assumptions to be valid: (1) low temperatures (dominance of Type I and Type II twins), (2) random c-axis orientations of calcite, (3) homogenous strain, (4) coaxial deformation, (5) volume constancy, (6) low-porosity materials, and (7) low strain (<15%). If these conditions are not fully met, the underlying data set of the calculated strain tensor could be biased, modified, or random. Strain tensors were calculated from calcite e-twin data sets with the software package of Evans and Groshong (1994). The calcite twinning-strain data are presented as table S6.

Results

Field Relations. White Mountain is composed of Ordovician Bighorn Dolomite and Mississippian Madison Limestone that were thermally metamorphosed into marbles before emplacement of the Heart Mountain slide. This thermal metamorphism was associated with the intrusion of a diorite stock at ~49.8 Ma (Malone et al. 2014*a*). The lamprophyre diatreme dike is at the west end of White Mountain and is hosted in the Bighorn and Madison marble. The marbles are flat

lying near the base of the allochthon, where the lamprophyre has intruded, but are more complexly deformed and steeply dipping near the contact of the diorite stock. The marbles are crosscut by eight sub-vertical CUC injectites that occur as much as 120 m above the SE-dipping, 3-m-thick CUC basal layer that defines the base of the Heart Mountain slide (Craddock et al. 2012). Andesitic, basaltic, and clastic dikes also crosscut the marble and diorite stock. Lower-plate rocks at White Mountain are flat lying and un-metamorphosed basal Bighorn Dolomite and Cambrian Snowy Range Limestone (Craddock et al. 2000, 2009).

The west end of White Mountain contains steeply included volcanic and plutonic rocks that terminate along the basal detachment. The contact between the igneous rocks and the marble strikes N55°E, can be traced for ~3 km, and is ~300 m high. Whole-rock compositional analyses of the igneous series, including diorite (fresh, weathered, foliated), lamprophyre, lamprophyre breccia, and clinopyroxenite, are shown

in table S1. The diorite and granodiorite are locally foliated, and the diorite has a U-Pb zircon age of ~49.9 Ma and is therefore older than the zircons in the CUC injectites and basal layer (Malone et al. 2014a). The lamprophyre (fig. 4) has a brown, apha-nitic groundmass with numerous armored lapilli and, aside from being interlayered with the clinopyro-xenite, looks much like the CUC injectites but does not react with HCl. The lamprophyre margin also contains diorite, granodiorite, and minor andesite, all of which are crosscut by the lamprophyre brec-cia. Both units are crosscut by aragonite and zeolite veins. The lamprophyre is found only above the base of the slide and is allochthonous (fig. 3).

Lamprophyre Description. Lamprophyres are vol-canic peralkaline and ultrapotassic igneous rocks that initiate in the subcontinental lithospheric mantle at 6–8-GPa pressures and temperatures of 1300°C. As a result of volatile saturation, they have an enormous pressure differential during ascent, similar to that of kimberlites (70 GPa; e.g., MacGregor 1970; Mitchell
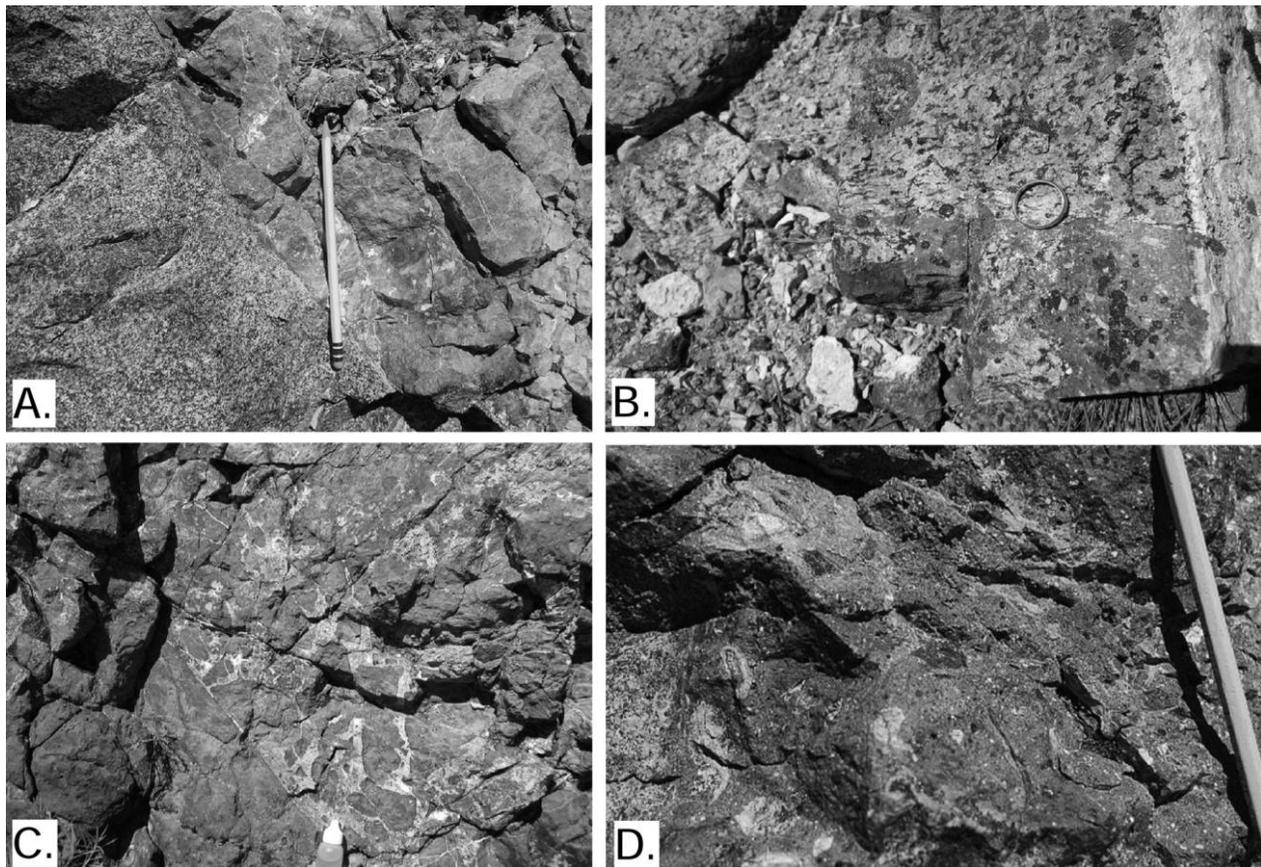
Figure 4. Field photographs of the White Mountain lamprophyre and related rocks. *A*, Lamprophyre (top) intruding diorite; *B*, foliated diorite; *C*, brecciated clinopyroxenite; and *D*, lamprophyre. A color version of this figure is available online.
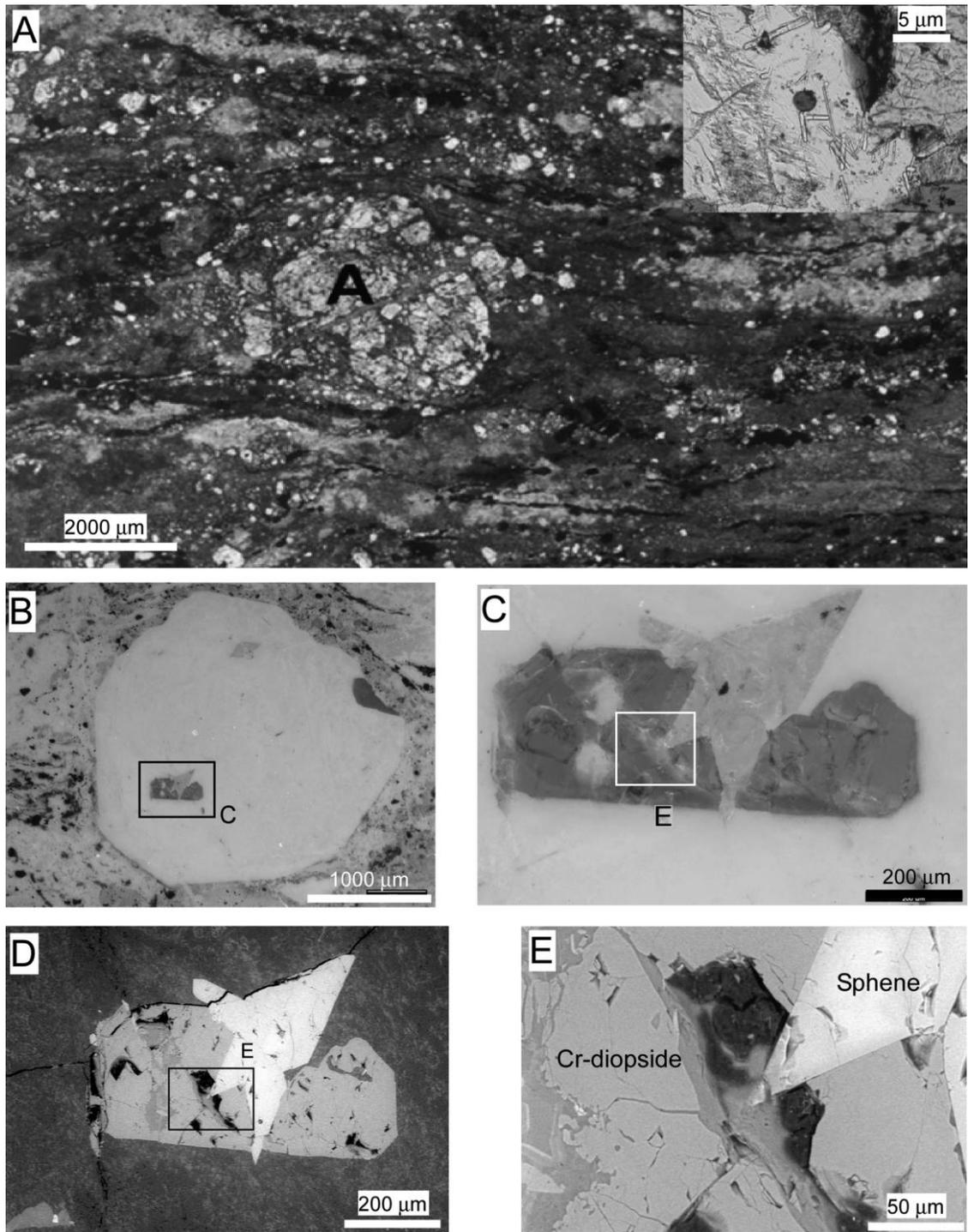
Figure 5. Photomicrographs of the White Mountain lamprophyre breccia. *A*, Foliated nature of the breccia (sample 11WY-55) from which the euhedral zircons were extracted (cathodoluminescence image, inset). *B, C*, Thin section of analcime (white) with inclusions of sphene (lighter inclusion in *C*), Cr-diopside (darker inclusions in *C*), and diamond (darkest areas in *E*) in plane light. *D*, Scanning electron microscopy backscatter image of *C*. *E*, Magnified view of diamond with Raman spectra spots. A color version of this figure is available online.
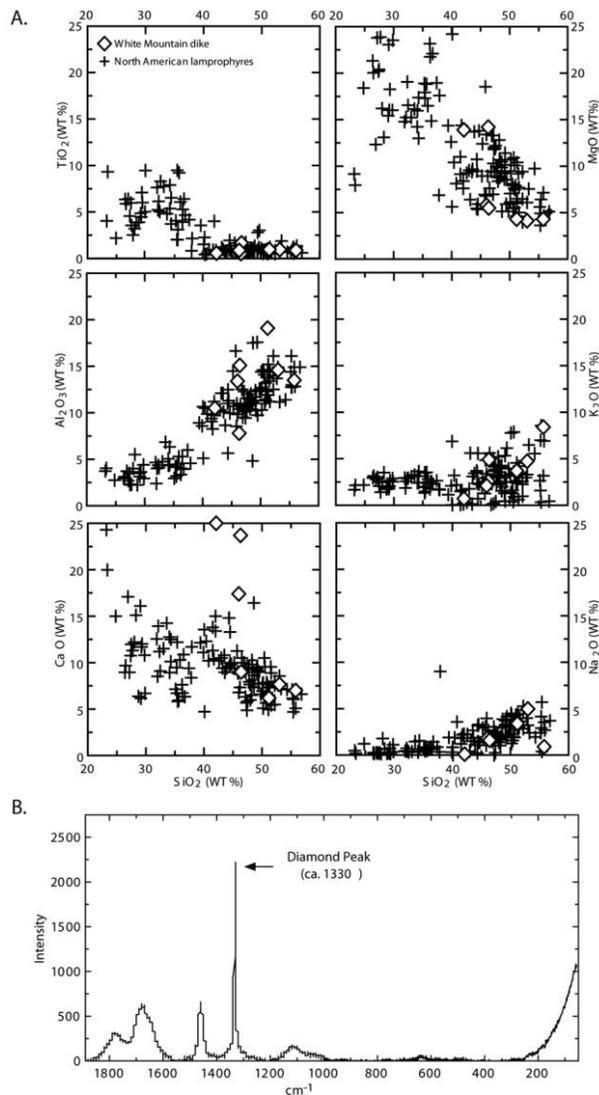
Figure 6. *A*, Major-element oxides from the White Mountain lamprophyre (diamonds) and published North American lamprophyres (plus signs). North American lamprophyre data compiled from the GEOROC (GEOchemistry of Rocks of the Oceans and Continents) database (Cullers and Medaris 1977; Laughlin et al. 1986; LeCheminant et al. 1987; Sage 1987; Wyman and Kerrich 1989, 1993; Barrie and Shirey 1991; Fitton et al. 1991; Wyman et al. 1995; Hattori et al. 1996; Sevigny and Thériault 2003; Tappe et al. 2004, 2008). *B*, Laser Raman spectroscopy of diamonds present in figure 5.

loss-on-ignition values (~30%; see CUC injectite XRF data in Craddock et al. 2012), whereas the lamprophyre breccia is SiO_2 rich (46%) and CaO rich (24%) and ultramafic in composition. The lamprophyre breccia contains olivine (forsterite), Cr-diopside, chromite, pyrope garnet, sphene, spinel, zircon, apatite, and secondary aragonite and analcime. Heavy-mineral separations yield significant amounts of pyrite, magnetite, ilmenite, and hematite, plus euhedral, weakly zoned zircons. The lamprophyre breccia contains euhedral, single-phase zircons, whereas many of the zircons in the CUC are rounded and polished and found with euhedral spinel. The breccia textures are chaotic but weakly foliated, with mantled lapilli, pyroxene with apatite needles, and rolled analcime clasts with included Cr-diopside, sphene, and diamonds (fig. 5). The diamonds (30–50 μm in diameter) are found in green clinopyroxenite and are pink in color. Raman spectroscopy (fig. 6) identifies a 1301-nm diamond peak, confirmed by ion microprobe and in situ X-ray diffractometry ($2\theta = 47.7°$ and 90°).

Whole-rock compositional analyses yielded results comparable to those for other North American lamprophyres (fig. 6; Cullers and Medaris 1977; Laughlin et al. 1986; LeCheminant et al. 1987; Sage 1987; Wyman and Kerrich 1989, 1993; Barrie and Shirey

and Bergman 1991; Heaman et al. 2004; Skinner and Marsh 2004; Sparks et al. 2006; Wilson and Head 2007; Cas et al. 2008).

The lamprophyre breccia at White Mountain was initially thought to be a CUC injectite (Malone et al. 2014*a*) until thin sections, heavy-mineral analysis, and XRF data became available. The CUC injectites are SiO_2 poor (7%) and CaO rich (38%) and have large
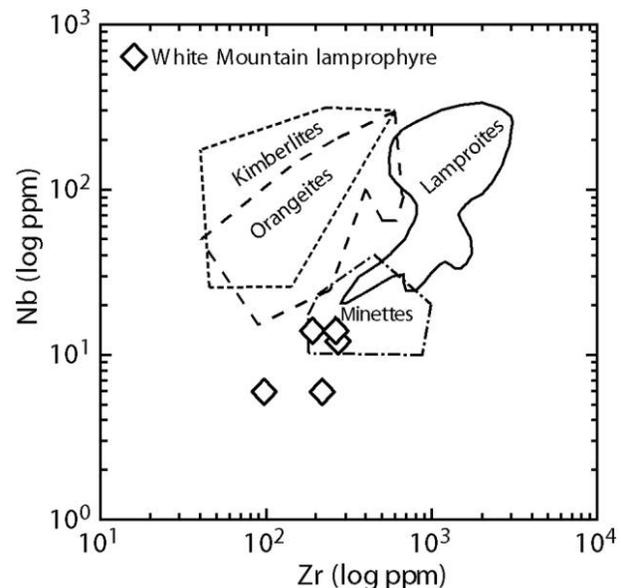
Figure 7. Log Zr-versus-Nb (ppm) plot comparing the White Mountain lamprophyre to alkaline igneous rocks in Montana. The plot shows that the White Mountain lamprophyre resembles a subtype of lamprophyre called a minette. Diagram after Hearn (2004), with lamprophyre and minette fields from Mitchell and Bergman (1991) and kimberlite and orangeite fields from Mitchell (1995).

1991; Fitton et al. 1991; Wyman et al. 1995; Hattori et al. 1996; Sevigny and Thériault 2003; Tappe et al. 2004, 2008). With the exception of CaO, all other major elements fit within the compositional ranges of published North American lamprophyre data. The high CaO values may be a result of a sampling bias, with disproportionately high clinopyroxene within the sample. Trace elements Zr and Nb show that the rocks from White Mountain are similar to minettes (fig. 7), which are associated with arc magmatism (Hearn 2004). Compositional and petrologic evidence suggests that the rocks on White Mountain are likely a diamond-bearing lamprophyre and that the rocks likely originated from the subcontinental lithospheric mantle.

Geochronology. Lamprophyre breccia–derived zircons are euhedral, without older cores, and were originally dated at 48.9 ± 0.5 Ma, as part of sample 11WY-55 (White Mountain injectite, as reported by Malone et al. 2014*a*), with LA-ICPMS techniques at the University of Arizona Laserchron Center. Sample 11WY-55 included zircons separated from several CUC injectites. As zircons for each individual injectite dike were sparse, the data from the set of dikes were compiled, and a resultant age was de-

termined. Sample 11WY-55 also contained zircons separated from the lamprophyre diatreme. These same zircon crystals were reoccupied with laser spot analyses for a suite of trace elements including REEs, Y, Ti, Nb, Ta, Hf, Th, and U. Figure 8 illustrates the trace-element concentrations of lamprophyre breccia zircons and Orapa kimberlite megacryst, superimposed on the compositions of a diverse suite of igneous zircons from Belousova et al. (2002). The trace-element compositions of the Orapa kimberlite zircon megacryst clearly overlap the distinctive fields of kimberlite zircon geochemistry defined by Belousova et al. (2002), typified by relatively high Hf contents, low REE and U contents, low Nb/Ta, and the lack of a Eu anomaly in the REE pattern. Compared to kimberlitic zircons, the lamprophyre breccia zircons span a larger range of correlated temperatures and Eu anomalies, indicative of magmatic differentiation in the presence of feldspar. The lamprophyre breccia zircons are clearly distinct from kimberlite zircon compositions, with higher REE contents, a minor negative Eu anomaly, and higher U contents and Nb/Ta. The geochemical characteristics of the lamprophyre breccia zircons do, however, overlap the compositions of lamproite zircon from Belousova
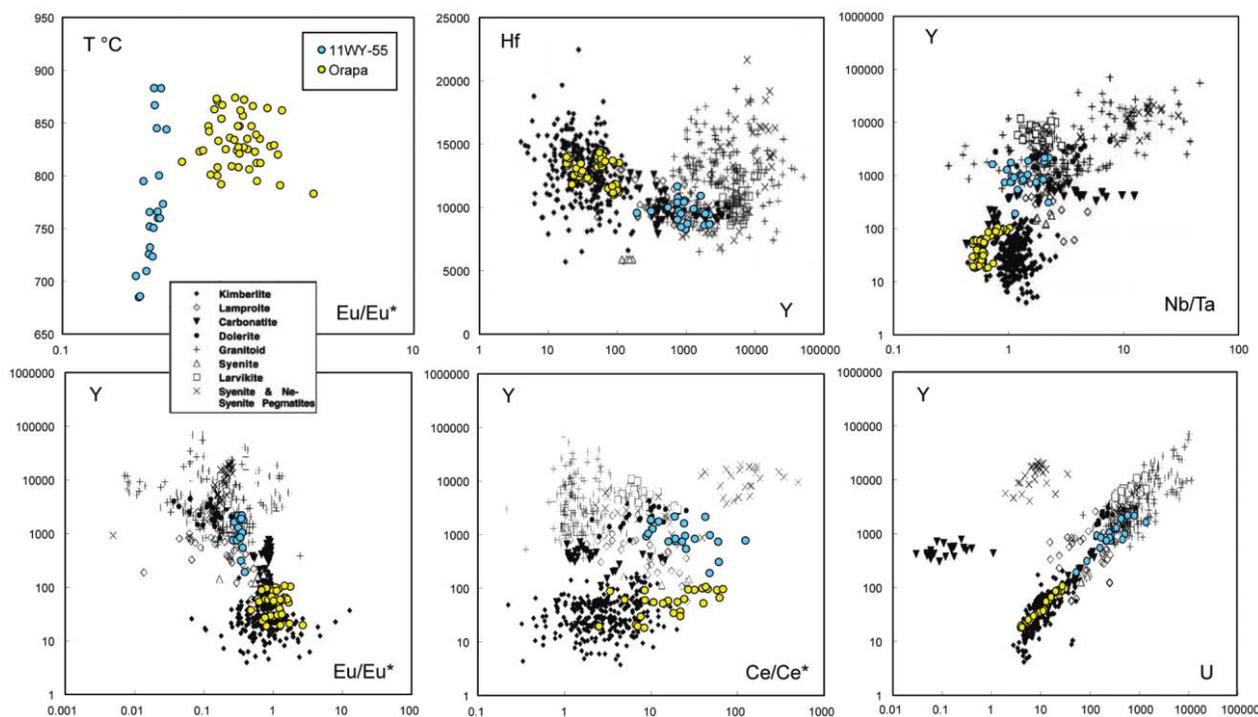
Figure 8. Trace-element geochemistry of lamprophyre breccia zircon crystals with respect to measurements of the Orapa kimberlitic zircon megacryst, and the ranges of compositions for a diverse suite of igneous zircons from Belousova et al. (2002). The compositions of the Orapa kimberlite and White Mountain lamprophyre zircons are themselves distinct but overlap the fields of kimberlite and lamproite zircon, respectively, from Belousova et al. (2002).
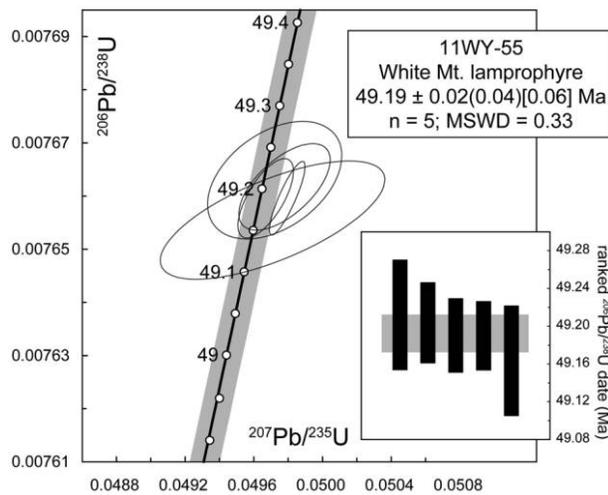
Figure 9. U-Pb concordia and ranked-age plots of chemical abrasion–isotope dilution TIMS results for zircons from lamprophyre breccia sample 11WY-55. The 49.19 ± 0.02 Ma date significantly refines the age of lamprophyre intrusion and is within the error of the 48.9 ± 0.5 age for carbonate ultracataclasite zircons at Silver Gate (Malone et al. 2014a).

et al. (2002), being less trace element enriched than most granitoid zircons.

On the basis of cathodoluminescence imagery and LA-ICPMS results, a selection of five grains were plucked from the epoxy mounts and analyzed via CA-IDTIMS. All grains yielded concordant and equivalent isotope ratios with a weighted mean $^{206}Pb/^{238}U$ date of 49.19 ± 0.02(0.04)[0.06] Ma (fig. 9). Given the consistency of this result and the simplicity of the zoning and compositions of this population of zircons, we interpret this result as estimating, within its analytical uncertainty, the emplacement age of the lamprophyre diatreme.

Rock Fabrics. Anisotropy of magnetic susceptibility (AMS) is a sensitive magnetic technique used as a proxy for measuring magmatic flow. Craddock et al. (2009) report a subhorizontal flow fabric (NW-SE) in the CUC basal layer, and we report here the results of AMS measurements in four CUC injectites and the lamprophyre (fig. 10; table S5). White Mountain injectites 1, 2, and 4 (fig. 2) represent one sample each from the vertical base of the structure, and injectite 3 has results from the bottom, middle, and top spanning ~100 m of relief. We also have one sample from the injectite at Silver Gate, 50 km to the northwest. There is no flow fabric in any of the CUC injectite AMS results except the top of White Mountain injectite 3, where the K_{max} values are all subvertical and the K_{min} values are subhorizontal and normal to the injectite. The AMS results for the

lamprophyre preserve a K_{max} flow fabric parallel to the lamprophyre dike (N55°E, 90°).

Additional oriented marble and vein samples were collected from White Mountain to complement the calcite strain results in Craddock et al. (2009; fig. 11; table S6). Samples 2a (marble) and 5 (limestone) preserve the pre–Heart Mountain layer–parallel shortening strain of the Sevier orogeny (Craddock and van der Pluijm 1989; Craddock et al. 2000). Sample 5 remained autochthonous with the E-W shortening orientation, whereas sample 2a has been rotated about a vertical axis by the landslide. Sample 6 is a calcite vein discovered in the footwall of White Mountain (N-S, 90°) that is truncated by the detachment and preserves a preslide horizontal shortening
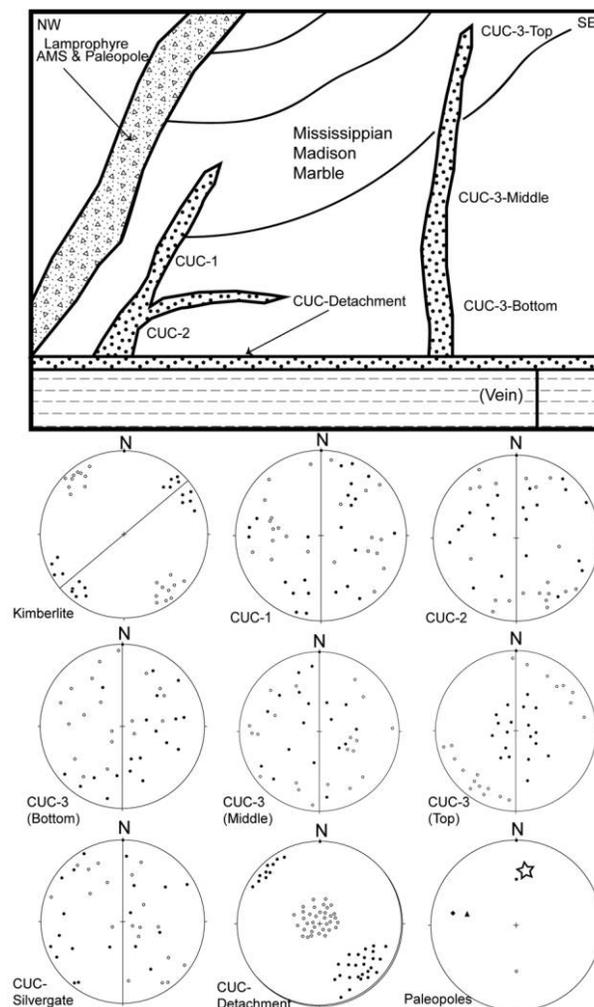
Figure 10. Lower-hemisphere projections of AMS (anisotropy of magnetic susceptibility) data (filled circles are for K_{max}, open circles for K_{min}; large circles illustrate orientations of the lamprophyre, injectites, or detachment). See figure 2 for sample locations and table S5, available online, for a summary. CUC = carbonate ultracataclasite.
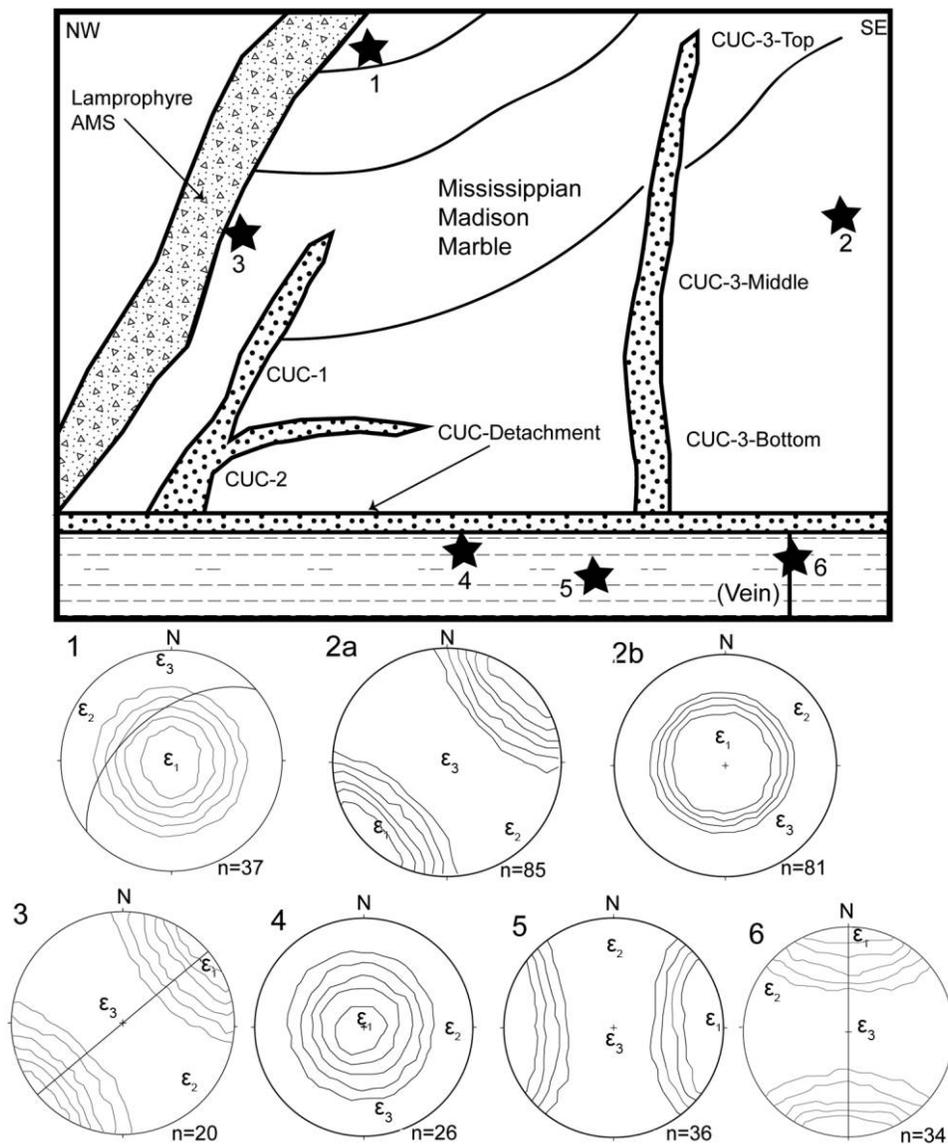
Figure 11. Schematic cross section of White Mountain and calcite twinning-strain data (table S6) plotted on lower-hemisphere projections (ε_1 = shortening axis; ε_2 = intermediate axis; ε_3 = extension axis). Sample details: 1. Madison Formation marble in contact with lamprophyre; 2a. Madison marble with pre–Heart Mountain layer–parallel shortening (N50°E); 2b. vertical-shortening overprint (negative expected values); 3. calcite vein parallel to the lamprophyre margin; 4. vertical shortening in detachment-parallel vein; 5. Pre–Heart Mountain layer–parallel shortening in footwall limestones; and 6. Laramide shortening in a vein truncated by the slide. AMS = anisotropy of magnetic susceptibility); CUC = carbonate ultracataclasite.

strain parallel to the vein with no strain overprint. Sample 1 is Madison Group marble (N55°E, 55°NW) in contact with the lamprophyre margin, sample 2b is the strain overprint (NEV) from the marble of sample 2a, and sample 4 is a detachment-parallel calcite vein; all three record a vertical shortening strain related to postslide burial. Differential stress magnitudes are remarkably consistent (−35 MPa) for twinning events that were tectonic or related to postslide burial. Electron backscatter diffractometry was measured on the basal CUC ($n = 183$) in contact with

Bighorn Dolomite ($n = 169$); neither material preserves an optic axis fabric (fig. 12).

Discussion

Enigmatic White Mountain, with its allochthonous marbles and its comparatively thick basal layer (2 m of CUC), now reveals additional information regarding the initiation and dynamics of the Eocene Heart Mountain slide. Detailed field mapping has documented the eight CUC injectites, which be-
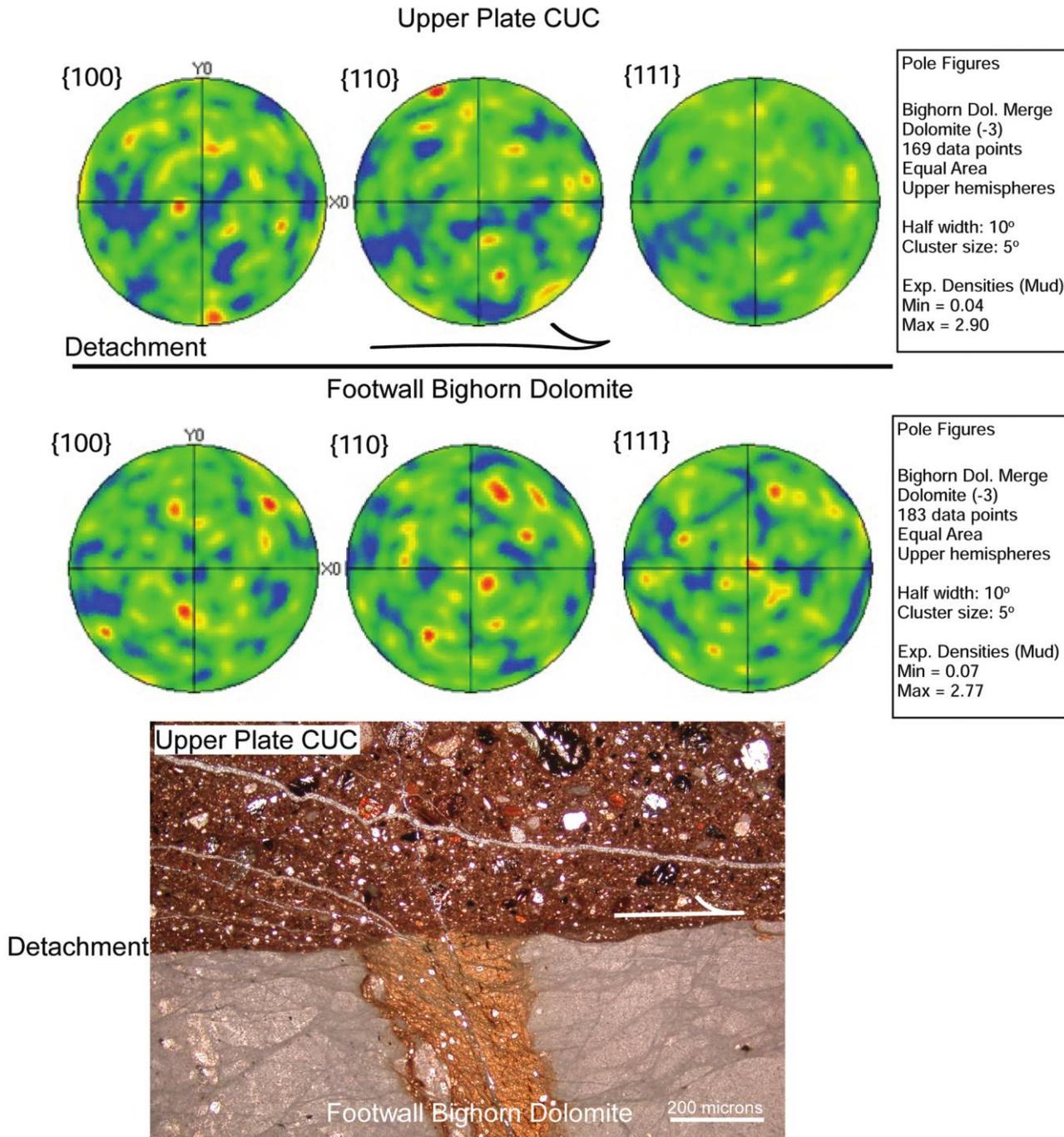
Figure 12. Electron backscatter diffraction pole results for the CUC (carbonate ultracataclasite; *top*) and Bighorn Dolomite (*bottom*) contact.

come listric (and/or join) with the basal CUC, and the presence of older intrusions (diorite, granodiorite; 49.9 ± 0.5 Ma) and the younger lamprophyre suite (breccia, clinopyroxenite, lamprophyre). Zircons in the lamprophyre breccia and CUC (injectites and basal layer; Malone et al. 2014*a*) are the same age (49.19 Ma ± 0.02 Ma TIMS age) and are

thereby also genetically and dynamically related. We suggest that the emplacement of the lamprophyre diatreme was the triggering mechanism for the catastrophic Heart Mountain slide and that White Mountain represents a remnant of the eruption center.

Eruption and Landslide Dynamics. Figures 13 and 14 portray the interpreted sequence of events at
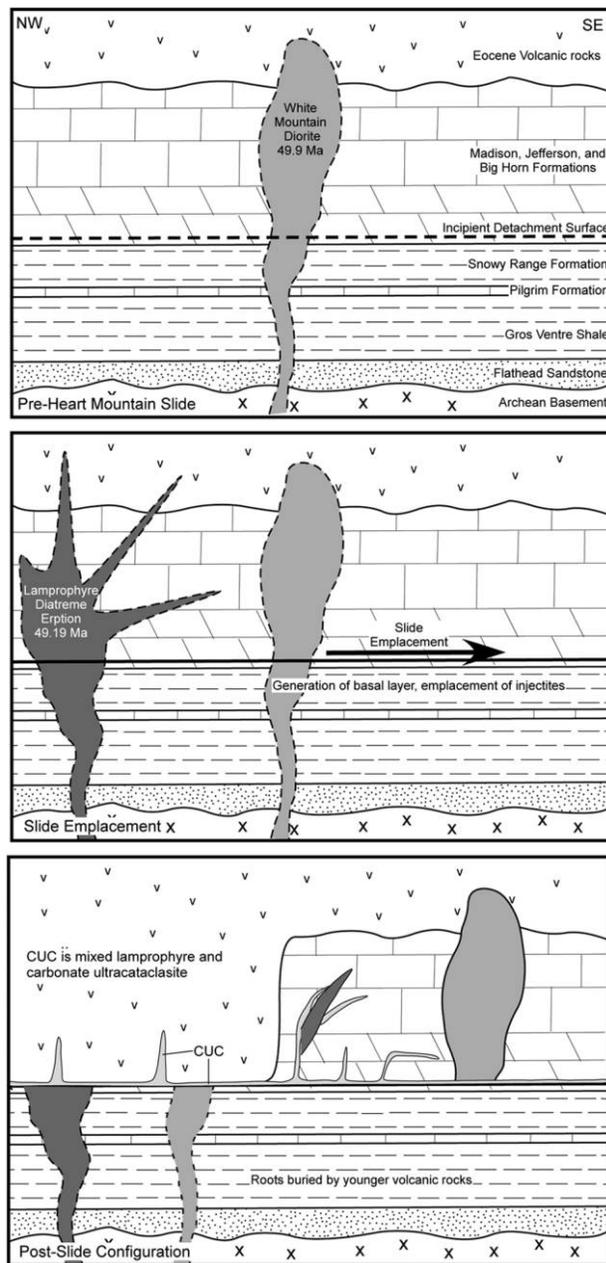
Figure 13. Schematic sequence of events at White Mountain (modified from Malone et al. 2014*a*; not to scale). Before the initiation of the Heart Mountain slide, a diorite stock intruded a succession of Paleozoic carbonate and Eocene volcanic rocks at ~49.9 Ma. The emplacement of a lamprophyre intrusion at ~49.19 Ma caused failure and collapse of the upper plate. This slab was catastrophically emplaced to the south and east into the adjacent Bighorn and Absaroka Basins. The basal layer carbonate ultracataclasite (CUC) contains cataclastic carbonate material derived from the upper plate, euhedral and abraded zircons from the lamprophyre and other intrusions, and delicate volcanic glass.

White Mountain. The diorite-granodiorite intruded at 49.9 ± 0.5 Ma and thermally metamorphosed the host carbonate rocks. The lamprophyre diatreme intrusion at 49.19 ± 0.02 Ma is preserved as a dike oriented at N55°E, 90°. The lamprophyre dike pinches out to the northeast, suggesting that the west end of the dike was connected to the main diatreme body. The lamprophyre diatreme intrusion, which triggered the emplacement of the Heart Mountain slide, included generation of the CUC fault gouge and injection (<120 m) of CUC into the upper plate. The AMS proxy for magmatic flow preserves a southeastward, subhorizontal flow in the CUC basal layer (Craddock et al. 2009) and chaotic flow in the injectites, except at the top of injectite 3. The lamprophyre AMS results suggest intrusion to the northeast (N55°E), as the K_{max} directions are subhorizontal and parallel to the intrusion. This AMS flow proxy is also parallel to the pre–Heart Mountain slide layer–parallel shortening strain preserved in the host Mississippian Madison limestones, which were oriented N90°E (Craddock et al. 2000) before the landslide. This means that the lamprophyre erupted in an E-W direction and then slid down the bedding-plane portion of the slide to its resting place at White Mountain (N55°E), which requires a horizontal rotation about a vertical axis and a minimum of 35° of counterclockwise motion. Alternatively, the White Mountain allochthon could have rotated to N55°E early in its motion and slid into place heading to the southeast, as the detachment striations and AMS fabric (K_{max}) at White Mountain trend S40°E.

Gentle N-S folds are present in the marble of western White Mountain. The marbles are terminated against the lamprophyre suite and preserve a vertical shortening strain. The lamprophyre-margin sheared calcite vein preserves a horizontal shortening strain parallel to the lamprophyre dike and no strain overprint; this is presumably deformation related to shearing along the lamprophyre margin during emplacement (fig. 11). Preslide calcite veins preserve a Laramide shortening strain (Craddock and van der Pluijm 1989) and no strain overprint. The marbles away from the lamprophyre preserve a vertical shortening-strain overprint (NEVs), and the coeval vein preserves vertical shortening; these are both interpreted to be related to postslide burial by younger Eocene volcanic rocks.

The lower-plate (subsurface) location of the lamprophyre diatreme is unknown and presumed to be west or northwest of White Mountain. The lamprophyre and CUC along the base of the slide and associated injectites were part of the same intrusion-landslide collapse event, as their zircons are the same age.
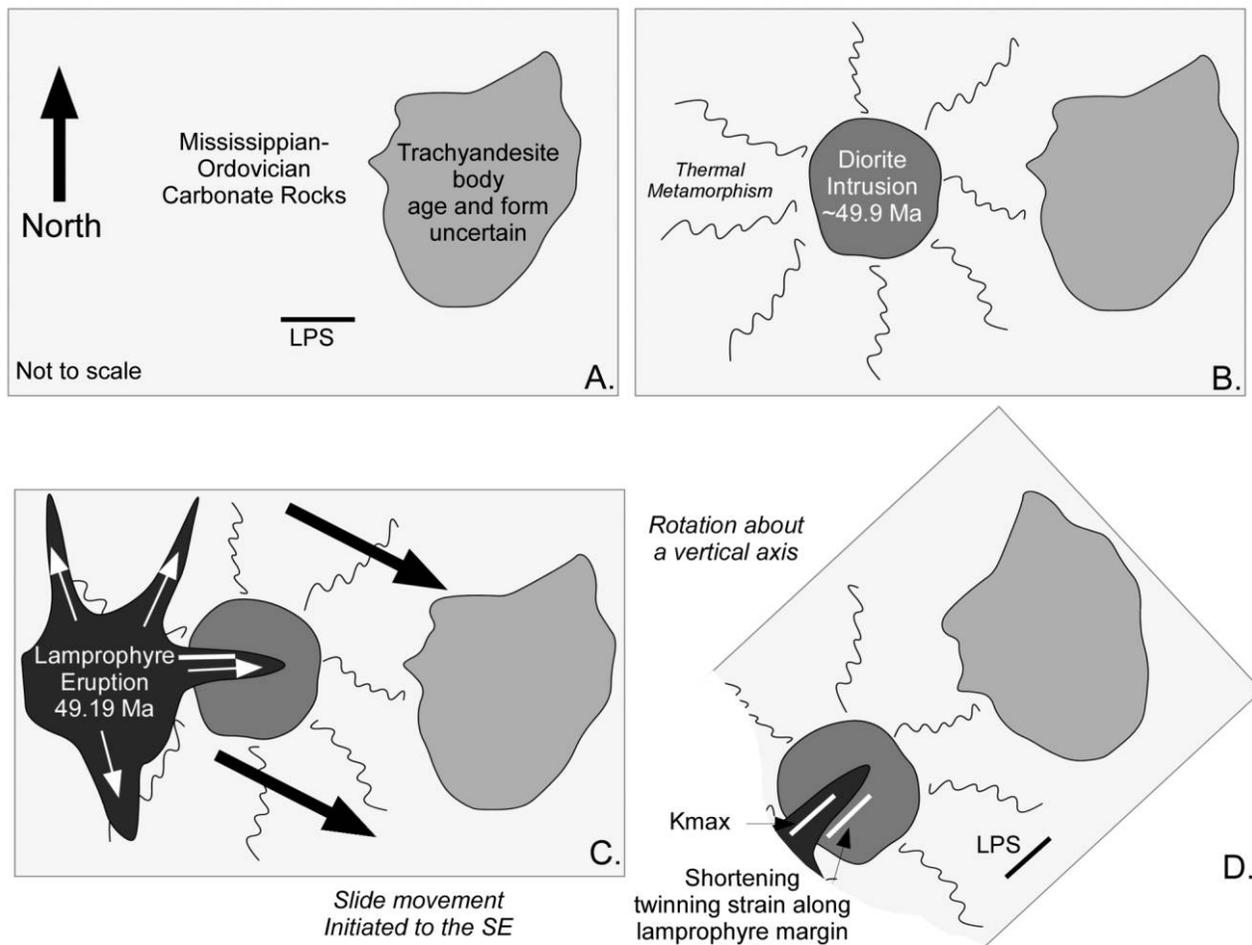
Figure 14. Map view schematic of the sequence of events at White Mountain. These diagrams are not to scale; the area shown is 5–10 km². At ~50 Ma, trachyandesite lavas and other volcanic rocks were deposited on Paleozoic carbonate rocks. The carbonate rocks preserve the Sevier Laramide E-W layer parallel strain. A diorite stock was emplaced at ~49.9 Ma. At ~49.19 Ma, during eruption, a lamprophyre diatreme intruded the diorite stock and host carbonate rock, with a K_{max} flow direction parallel to the to the Sevier-Laramide E-W layer parallel strain. The eruption caused the upper plate to fail, and the allochthonous rocks at White Mountain were transported to the southeast while rotating counterclockwise about a vertical axis of rotation, before coming to rest at their current location. LPS = layer-parallel shortening.

Regional Field Relations. Heart Mountain and McCullough Peaks are the most obvious and distal upper-plate slide blocks of Madison Group limestones in the Bighorn Basin. It is now apparent that the vertical volcaniclastic rocks atop Squaw Peaks in the southern Bighorn Basin are also part of the Heart Mountain slide run-out, along with Eocene volcanic rocks in the upper South Fork Shoshone River Valley and Carter Mountain (Malone 1995, 1996, 1997; Malone et al. 2014b, 2014c). The Absaroka volcanic field covers an area of ~8,000 km² with a composite thickness of ~5 km extruded between 55 and 38 Ma (Sundell 1993). This extensive mafic-intermediate outpouring may in some way be related to Eocene rollback of the Farallon Plate

(Humphreys 1995; Smith et al. 2014) and is an anomalous thick, horizontal cap in northwest Wyoming, especially when compared to the variety of other alkaline Eocene intrusions in the area (Sundell 1993; Feeley and Cosca 2003)

CO₂ Generated by the Heart Mountain Slide. The emplacement of the Heart Mountain slide has been proposed to be the result of a reduction in friction along the detachment, perhaps accommodated by CO and CO_2 generated by limestone-on-limestone sintering (Han et al. 2007; Mitchell et al. 2015) and the introduction of mantle CO and CO_2 when the lamprophyre erupted. We have calculated the amount of CO_2 generated by the Heart Mountain slide to be 7 billion kilograms (0.07 gigatons), which is a mi-

nuscule amount of CO_2 when compared to the annual human (29 gigatons) and oceanic (332 gigatons) CO_2 emissions. The observation and interpretation that a lamprophyre eruption occurred and triggered the event provides an answer to the question, what caused this slab of rock to move to begin with? Once the emplacement was triggered, the various mechanisms suggested by Beutner and Gerbi (2005), Aharonov and Anders (2006), Craddock et al. (2009), and Anders et al. (2010) that aided continued movement may have operated.

Conclusions

Our understanding of the Heart Mountain slide has been refined during the past decades. There are now data for (1) the structure and stratigraphy of the rocks involved (Pierce 1973; Malone 1995, 1996, 1997), (2) emplacement duration (Craddock et al. 2000, 2009), (3) emplacement timing (Malone et al. 2014*a*; this report), (4) areal extent (Malone et al. 2014*b*, 2014*c*), (5) the relationship between the South Fork and Heart Mountain slide masses (Craddock et al. 2015), (6) the characteristics of the CUC (Beutner and Craven 1996; Beutner and Gerbi 2005, Craddock et al. 2009, 2012; Anders et al. 2010), and (7) the regional paleogeography at the time of collapse (Rhodes et al. 2007; Malone et al. 2014*b*, 2014*c*; Craddock et al. 2015).

White Mountain, with its allochthonous marble, has always been an anomaly within the chaos of the Heart Mountain slide. We argue that the marble is the result of contact metamorphism adjacent to an older diorite intrusive suite and that the younger lamprophyre was the triggering mechanism for the volcanically induced landslide at ~49.19 Ma. Zircons in the lamprophyre breccia and resultant CUC (basal layer and injectites) are the same age and thereby genetically related. A supersonic lamprophyre eruption helps explain earlier computations about the mechanism and rapid initiation speed (100 m/s) of the landslide, which also makes plausible the increase in the chaotic, rotational run-out

of the slide (~5000 km²) to include the Eocene volcaniclastic rocks at Squaw Peaks and Hominy Peak (100 km to the west). The location of the lamprophyre root remains unknown but is presumed to be upgradient to the west of White Mountain and is part of the regional grouping of Cretaceous-Eocene alkaline and ultramafic intrusions that intruded as the Farallon slab rolled back to the southwest between 50 and 45 Ma.

It is interesting that we may have come full circle with respect to an explanation for the initiation of the Heart Mountain slide. Bucher (1933) was the first to suggest that Heart Mountain was propelled to the east by a gigantic volcanic explosion. His explanation was

The writer thinks it possible that the limestone-plates which constitute the thrust-masses of this region were thrust eastward and scattered much as they are today by the horizontal component of the force of a large volcanic explosion . . . volcanic gases, perhaps largely pent-up steam, exploded in such a way as to shear off large sheets of limestone from the highly micaceous Cambrian shales and to drive them eastward (or, perhaps better, southeastward) down the pediment slope into the plain.

REFERENCES CITED

Aharonov, E., and Anders, M. H. 2006. Hot water: a solution to the Heart Mountain detachment problem? Geology 34:165–168.

Anders, M. H.; Fouke, B. W.; Zerkle, A. L.; Tavarnelli, E.; Alvarez, W.; and Harlows, G. E. 2010. The role of calcining and basal fluidization in the long runout of carbonate slides: an example from the Heart Mountain

Slide Block, Wyoming and Montana, U.S.A. J. Geol. 118:577–599.

Barrie, C. T., and Shirey, S. B. 1991. Nd- and Sr-isotope systematics for the Kamiskotia-Montcalm area: implications for the formation of late Archean crust in the western Abitibi Subprovince, Canada. Can. J. Earth Sci. 28:58–76.

Belousova, E.; Griffin, W. L.; O'Reilly, S. Y.; and Fisher, N. L. 2002. Igneous zircon: trace element composition as an indicator of source rock type. Contrib. Mineral. Petrol. 143:602–622.

Beutner, E. C., and Craven, A. E. 1996. Volcanic fluidization and the Heart Mountain detachment, Wyoming. Geology 24:595–598.

Beutner, E. C., and Gerbi, G. P. 2005. Catastrophic emplacement of the Heart Mountain block slide, Wyoming and Montana, USA. Geol. Soc. Am. Bull. 117: 724–735.

Bucher, W. H. 1933. Problem of the Heart Mountain thrust [abs.]: Proc. Geol. Soc. Am. p. 57.

———. 1947. Heart Mountain problem. *In* Blackstone, D. L., Jr., and Sternberg, C. W., eds. Field conference in the Bighorn Basin: guidebook. Casper, Wyo. Geol. Assoc., p. 189–197.

Burkhard, M. 1993. Calcite twins, their geometry, appearance and significance as stress-strain markers and indicators of tectonic regime: a review. J. Struct. Geol. 15:351–368.

Cas, R. A. F.; Hayman, P.; Pittari, A.; and Porritt, L. 2008. Some major problems with existing models and terminology associated with kimberlite pipes from a volcanological perspective, and some suggestions. J. Volcanol. Geotherm. Res. 174:209–225.

Condon, D. J.; Schoene, B.; McLean, N. M.; Bowring, S. A.; and Parrish, R. R. 2015. Metrology and traceability of U–Pb isotope dilution geochronology (EARTHTIME tracer calibration part I). Geochim. Cosmochim. Acta 164:464–480.

Craddock, J. P.; Anziano, J.; Wirth, K. R.; Vervoort, J. D.; Singer, B.; and Zhang, X. 2007. Structure, geochemistry and geochronology of a kimberlite dike swarm, Archean Wawa terrane, Michigan, USA. Precambrian Res. 157:50–70.

Craddock, J. P.; Farris, D.; and Roberson, A. 2004. Calcite-twinning constraints on stress-strain fields along the Mid-Atlantic Ridge, Iceland. Geology 32:49–52.

Craddock, J. P.; Geary, J.; and Malone, D. H. 2012. Vertical injectites of detachment carbonate ultracataclasite at White Mountain, Heart Mountain detachment, Wyoming. Geology 40:463–466.

Craddock, J. P.; Malone, D. H.; Cook, A. L.; Rieser, M. E.; and Doyle, J. R. 2009. Dynamics of emplacement of the Heart Mountain allochthon at White Mountain: constraints from calcite twinning strains, anisotropy of magnetic susceptibility and thermodynamic calculations. Geol. Soc. Am. Bull. 121:919–938.

Craddock, J. P.; Malone, D. H.; MacNamee, A. F.; Mathisen, M.; Leonard, A. M.; and Kravits, K. 2015. Structural evolution of the Eocene South Fork slide, northwest Wyoming. J. Geol. 123:311–335.

Craddock, J. P.; Moshoian, A.; and Pearson, A. M. 1991. Kinematic analysis from twinned calcite strains in the marble mylonites of the central Grenville province, Canada. Geol. Soc. Am. Abstr. Program 15:236.

Craddock, J. P.; Nielson, K. J.; and Malone, D. H. 2000. Calcite twinning strain constraints on Heart Moun-

tain detachment kinematics, Wyoming. J. Struct. Geol. 22:983–991.

Craddock, J. P., and Pearson, A. 1994. Non-coaxial horizontal shortening strains preserved in amygdule calcite, DSDP Hole 433C, Suiko Seamount. J. Struct. Geol. 16:719–724.

Craddock, J. P.; Pearson, A.; McGovern, M.; Kropf, E. P.; Moshoian, A.; and Donnelly, K. 1997. Post-extension shortening strains preserved in calcites of the Keweenawan rift. *In* Ojakgangas, R. W.; Dickas, A. B.; and Green, J. C., eds. Middle Proterozoic to Cambrian rifting, central North America. Geol. Soc. Am. Spec. Pap. 312:115–126.

Craddock, J. P., and van der Pluijm, B. A. 1988. Kinematic analysis of an en échelon–continuous vein complex. J. Struct. Geol. 10:445–452.

———. 1989. Late Paleozoic deformation of the cratonic carbonate cover of eastern North America. Geology 17:416–419.

Cullers, R. L., and Medaris, G., Jr. 1977. Rare earth elements in carbonatite and cogenetic alkaline rocks: examples from Seabrook Lake and Callander Bay, Ontario. Contrib. Mineral. Petrol. 65:143–153.

DeFrates, J.; Malone, D. H.; and Craddock, J. P. 2006. Anisotropic magnetic susceptibility (AMS) analysis of basalt dikes at Cathedral Cliffs, WY: implications for Heart Mountain faulting. J. Struct. Geol. 28:9–18.

Engelder, T. 1979. The nature of deformation within the outer limits of the central Appalachian foreland fold-and-thrust belt in New York state. Tectonophysics 55:289–310.

Evans, M. A., and Groshong, R. H., Jr. 1994. A computer program for the calcite strain-gage technique. J. Struct. Geol. 16:277–281.

Feeley, T. C., and Cosca, M. A. 2003. Time vs. composition trends of magmatism at Sunlight Volcano, Absaroka Volcanic Province, Wyoming. Geol. Soc. Am. Bull. 115:714–728.

Ferrill, D. A. 1991. Calcite twin widths and intensities as metamorphic indicators in natural low-temperature deformation of limestone. J. Struct. Geol. 13:675–677.

———. 1998. Critical re-evaluation of differential stress estimates from calcite twins in coarse-grained limestone. Tectonophysics 285:77–86.

Ferrill, D. A.; Morris, A. P.; Evans, M. A.; Burkhard, M.; Groshong, R. H., Jr.; and Onasch, C. M. 2004. Calcite twin morphology: a low-temperature deformation geothermometer. J. Struct. Geol. 26:1521–1529.

Fitton, J. G.; James, D.; and Leeman, W. P. 1991. Basic magmatism associated with late Cenozoic extension in the western United States: compositional variations in space and time. J. Geophys. Res. 96(B8):13,693–13,711.

Gray, M. B.; Stamatakos, J. A.; Ferrill, D. A.; and Evans, M. A. 2005. Fault-zone deformation in welded tuffs at Yucca Mountain, Nevada, USA. J. Struct. Geol. 27: 1873–1891.

Groshong, R. H., Jr. 1972. Strain calculated from twinning in calcite. Geol. Soc. Am. Bull. 83:2025–2038.

———. 1974. Experimental test of least-squares strain calculations using twinned calcite. Geol. Soc. Am. Bull. 85:1855–1864.

Groshong, R. H. Jr.; Teufel, L. W.; and Gasteiger, C. M. 1984. Precision and accuracy of the calcite strain-gage technique. Geol. Soc. Am. Bull. 95:357–363.

Hacker, D. B.; Biek, R. F.; and Rowley, P. D. 2014. Catastrophic emplacement of the gigantic Markagunt gravity slide, southwest, Utah (USA): implications for hazards associated with sector collapse of volcanic fields. Geology 42:943–946.

Han, R.; Shimamoto, T.; Hirose, T.; Ree, J.-H.; and Ando, J.-I. 2007. Ultralow friction of carbonate faults caused by thermal decomposition. Science 316:878–881.

Hattori, K.; Hart, S. R.; and Shimizu, N. 1996. Melt and source mantle composition in the late Archean: a study of strontium and neodymium isotope and trace elements in clinopyroxenes from shoshonitic alkaline rocks. Geochim. Cosmochim. Acta 60:4551–4562.

Hauge, T. A. 1985. Gravity-spreading origin of the Heart Mountain allochthon, northwestern Wyoming. Geol. Soc. Am. Bull. 96:1440–1456.

———. 1990. Kinematic model of continuous Heart Mountain allochthon. Geol. Soc. Am. Bull. 102:1174–1188.

———. 1993. The Heart Mountain detachment, northwestern Wyoming: 100 years of controversy. In Snoke, A. W.; Steidtman, J. R.; and Roberts, S. M., eds. Geology of Wyoming. Wyo. Geol. Surv. Mem. 5:530–571.

Heaman, L. M.; Kjarsgaard, B. A.; and Creaser, R. A. 2004. The temporal evolution of North American kimberlites. Lithos 76:377–397.

Hearn, B. C., Jr. 2004. The Homestead kimberlite, central Montana, USA: mineralogy, xenocrysts, and upper-mantle xenoliths. Lithos 77:473–491.

Humphreys, E. D. 1995. Post-Laramide removal of the Farallon slab, western United States. Geology 23:987–990.

Kilsdonk, W., and Wiltschko, D. V. 1988. Deformation mechanisms in the southeastern ramp region of the Pine Mountain block, Tennessee. Geol. Soc. Am. Bull. 100:644–653.

King, E. M.; Malone, D. H.; and DeFrates, J. 2009. Oxygen isotope evidence of heated pore fluid interaction with mafic dikes at Cathedral Cliffs, Wyoming. Mt. Geol. 46(3):1–18.

Lacombe, O., and Laurent, P. 1996. Determination of deviatoric stress tensors based on inversion of calcite twin data from experimentally deformed monophase samples: preliminary results. Tectonophysics 255:189–202.

Laughlin, A. W.; Aldrich, M. J.; Squafiquallah, M.; and Husler, J. W. 1986. Tectonic implications of the age, composition, and orientation of kimberlite dykes, Navajo Volcanic field, Arizona. Earth Planet. Sci. Lett. 76:361–374.

LeCheminant, A. N.; Miller, A. R.; and LeCheminant, G. M. 1987. Early Proterozoic alkaline igneous rocks, district of Keewatin, Canada: petrogenesis and mineralization. In Pharaoh, T. C.; Beckinsale, R. D.; and Rickard, D., eds. Geochemistry and mineralization of Proterozoic volcanic suites. Spec. Publ. Geol. Soc. Lond. 33:219–240.

Ludwig, K. R. 2008. Isoplot 3.60. Spec. Publ. 4. Berkeley, CA, Berkeley Geochronology Center, 77 p.

MacGregor, I. D. 1970. An hypothesis for the origin of kimberlite. In Morgan, B. A.; Jones, B. F.; Kullerud, G.; Osborn, E. F.; and Holser, W. T., eds. Fiftieth anniversary symposia. Mineral. Soc. Am. Spec. Pap. 3:51–62.

Malone, D. H. 1995. A very large debris-avalanche deposit within the Eocene volcanic succession of the northeastern Absaroka Range, Wyoming. Geology 23:661–664.

———. 1996. Revised stratigraphy of Eocene volcanic rocks in the lower North and South Fork Shoshone River valleys, Wyoming. In Bowen, C. E.; Kirkwood, S. C.; and Miller, T. S., eds. Resources of the Bighorn Basin. 47th Annual Field Conference guidebook. Casper, Wyo. Geol. Assoc., p. 109–138.

———. 1997. Recognition of a distal facies greatly extends the domain of the Deer Creek Debris-Avalanche Deposit (Eocene), Absaroka Range, Wyoming. In McCutcheon, T. J., and McCutcheon, J. A., eds. Prospect to pipeline. 48th Annual Field Conference guidebook. Casper, Wyo. Geol. Assoc., p. 1–9.

Malone, D. H., and Craddock, J. P. 2008. Recent contributions to the understanding of the Heart Mountain detachment, Wyoming. Northwest Geol. 37:21–40.

Malone, D. H.; Craddock, J. P.; Anders, M. H.; and Wulff, A. P. 2014a, Constraints on the emplacement age of the massive Heart Mountain slide, northwestern Wyoming. J. Geol. 122:671–685.

Malone, D. H.; Craddock, J. P.; and Mathesin, M. G. 2014b. Origin of allochthonous volcanic rocks at Squaw Peaks, Wyoming: a distal remnant of the Heart Mountain slide? Mt. Geol. 51:321–336.

Malone, D. H.; Craddock, J. P.; and Schroeder, K. A. 2014c. Detrital zircon age and provenance of Wapiti Formation (Eocene) tuffaceous sandstones, South Fork Shoshone River Valley, Wyoming. Mt. Geol. 51:279–294.

Mitchell, R. H. 1995. Kimberlites, orangeites, and related rocks. New York, Plenum.

Mitchell, R. H., and Bergman, S. C. 1991. Petrology of lamproites. New York, Plenum.

Mitchell, T. M.; Smith, S. A.; Anders, M. H.; Di Toro, G.; Nielsen, S.; Cavallo, A.; and Beard, A. D. 2015. Catastrophic emplacement of giant landslides aided by thermal decomposition: Heart Mountain, Wyoming. Earth Planet. Sci. Lett. 411:199–207.

Mosar, J. 1989. Internal deformation in the Préalpes Médianes (Switzerland). Eclogae Geol. Helv. 82:765–793 (in French with English abstract).

Nelson, W. H., and Pierce, W. G. 1968. Wapiti Formation and Trout Peak trachyandesite, northwest Wyoming. U.S. Geol. Surv. Bull. 1254-H, 11 p.

Nelson, W. H.; Pierce, W. G.; Parsons, W. H.; and Brophy, G. P. 1972. Igneous activity, metamorphism, and Heart

Mountain faulting at White Mountain, northwestern Wyoming. Geol. Soc. Am. Bull. 83:2607–2620.

Paulsen, T. S.; Wilson, T. J.; Demosthenous, C.; Millan, C.; Jarrad, R.; and Laufer, A. 2014. Kinematics of the Neogene Terror rift: constraints from calcite twinning strains in the ANDRILL McMurdo Ice Shelf (AND-1B) core, Victoria Land Basin, Antarctica. Geosphere 10:828–841.

Pierce, W. G. 1973. Principal features of the Heart Mountain fault and the mechanism problem. In DeJong, K. A., and Scholten, R., eds. Gravity and tectonics. New York, Wiley, p. 457–471.

———. 1979. Clastic dikes of Heart Mountain fault breccia, northwestern Wyoming, and their significance. U.S. Geol. Surv. Prof. Pap. 1133, 25 p.

Rhodes, M. K.; Malone, D. H.; Carroll, A. R.; and Smith, M. 2007. Sudden desiccation of Lake Gosiute at 49 Ma: a downstream effect of Heart Mountain faulting? Mt. Geol. 44(1):1–10.

Rivera, T. A.; Storey, M.; Schmitz, M. D.; and Crowley, J. L. 2013. Age intercalibration of $^{40}Ar/^{39}Ar$ sanidine and chemically distinct U/Pb zircon populations from the Alder Creek Rhyolite Quaternary geochronology standard. Chem. Geol. 345:87–98.

Rowe, K. J., and Rutter, E. H. 1990. Paleostress estimation using calcite twinning: experimental calibration and application to nature. J. Struct. Geol. 12:1–17.

Sage, R. P. 1987. Geology of carbonatite-alkalic rock complexes in Ontario: Borden Township Carbonatite Complex, District of Sudbury. Ontario Geol. Surv. Study 33:1–62.

Sevigny, J. H., and Thériault, R. J. 2003. Geochemistry and Sr-Nd isotopic compositions of Eocene kimberlite dykes, southeastern British Columbia. Can. J. Earth Sci. 40:853–864.

Skinner, E. M. W., and Marsh, J. S. 2004. Distinct kimberlite pipe classes with contrasting eruption processes. Lithos 76:183–200.

Sláma, J.; Košler, J.; Condon, D. J.; Crowley, J. L.; Gerdes, A.; Hanchar, J. M.; and Schaltegger, U. 2008. Plešovice zircon—a new natural reference material for U-Pb and Hf isotopic microanalysis. Chem. Geol. 249:1–35.

Smith, M. E.; Carroll, A. R.; Jicha, B. R.; Cassel, E. J.; and Scott, J. J. 2014. Paleogeographic record of Eocene Farallon slab rollback beneath western North America. Geology 42:1039–1042.

Spang, J. H., and Groshong, R. H., Jr. 1981. Deformation mechanisms and strain history of a minor fold from the Appalachian Valley and Ridge Province. Tectonophysics 72:323–342.

Sparks, R. S. J.; Baker, L.; Brown, R. J.; Field, M.; Schumacher, J.; Stripp, G.; and Walters, A. 2006. Dynamical constraints on kimberlite volcanism. J. Volcanol. Geotherm. Res. 155:18–48.

Sundell, K. A. 1993. A geologic overview of the Absaroka volcanic province. In Snoke, A. W.; Steidtman, J. R.;

and Roberts, S. M., eds. Geology of Wyoming. Wyo. Geol. Surv. Mem. 5:480–506.

Swanson, E.; Wernicke, B. P.; and Hauge, T. A. 2016. Episodic dissolution, precipitation, and slip along the Heart Mountain detachment, Wyoming. J. Geol. 124: 75–97.

Tappe, S.; Foley, S. F.; Kjarsgaard, B. A.; Romer, R. L.; Heaman, L. M.; Stracke, A.; and Jenner, G. A. 2008. Between carbonatite and lamproite-diamondiferous Torngat ultramafic kimberlites formed by carbonate-fluxed melting of cratonic marid-type metasomes. Geochim. Cosmochim. Acta 72:3258–3286.

Tappe, S.; Jenner, G. A.; Foley, S. F.; Heaman, L. M.; Besserer, D.; Kjarsgaard, B. A.; and Ryan, B. 2004. Torngat ultramafic kimberlites and their relation to the North Atlantic Alkaline Province. Lithos 76:491–518.

Templeton, A. S.; Sweeney, J., Jr.; Manske, H.; Tilghman, J. F.; Calhoun, S. C.; Violich, A.; and Chamberlain, C. P. 1995. Fluids and the Heart Mountain fault revisited. Geology 23:929–932.

Teufel, L. W. 1980. Strain analysis of experimental superposed deformation using calcite twin lamellae. Tectonophysics 65:291–309.

Turner, F. J. 1953. Nature and dynamic interpretation of deformation lamellae in calcite of three marbles. Am. J. Sci. 251:276–298.

———. 1962. "Compression" and "tension" axes deduced from {0112} twinning in calcite. J. Geophys. Res. 67:1660.

Watson, E. B.; Wark, D. A.; and Thomas, J. B. 2006. Crystallization thermometers for zircon and rutile. Contrib. Mineral. Petrol. 151:401:413.

Wenk, H.-R.; Takeshita, T.; Bechler, E.; Erskine, B. G.; and Matthies, S. 1987. Pure shear and simple shear calcite textures. Comparison of experimental, theoretical and natural data. J. Struct. Geol. 9:731–745.

Wilson, L., and Head, J. W. 2007. An integrated model of kimberlite ascent and eruption. Nature 447:53–57.

Wiltschko, D. V.; Medwedeff, D. A.; and Millson, H. E. 1985. Distribution and mechanisms of strain within rocks on the northwest ramp of Pine Mountain block, southern Appalachian foreland: a field test of theory. Geol. Soc. Am. Bull. 9:426–435.

Wyman, D. A., and Kerrich, R. 1989. Archean lamprophyte dikes of the Superior Province, Canada: distribution, petrology, and geochemical characteristics. J. Geophys. Res. 94(B4):4667–4696.

———. 1993. Archean shoshonitic kimberlites of the Abitibi Subprovince, Canada: petrogenesis, age, and tectonic setting. J. Petrol. 34:1067–1109.

Wyman, D. A.; Kerrich, R.; and Sun, M. 1995. Noble metal abundances of late Archean (2.7 Ga) accretion-related shoshonitic kimberlites, Superior Province, Canada. Geochim. Cosmochim. Acta 59:47–57.